



Cite this: *J. Mater. Chem. C*, 2025,  
13, 14910

## Enhanced electrical properties and stability of solution processed IYZO thin film transistors by controlling deep level oxygen vacancies†

Bu Kyeong Hwang,<sup>a,b</sup> Hyeon Woo Kim,<sup>a,c</sup> Bo Ram Lee,<sup>a,b</sup> Eun Jin Park,<sup>a</sup> Hyunsung Jung,<sup>a</sup> Min-Kyu Son, Sung Beom Cho, <sup>b,d,e</sup> Hyeon Jin Jung,<sup>\*a</sup> Moonsuk Yi<sup>\*b</sup> and Soo Won Heo

In this study, ytterbium (Yb) was introduced as a dopant to improve the stability of indium–zinc oxide (IZO) thin film transistors (TFTs). The stability and electrical performance of indium–ytterbium–zinc oxide (IYZO) TFTs were compared with those of indium–gallium–zinc oxide (IGZO) TFTs with gallium (Ga) as a typical dopant. In particular, under a negative bias illumination stress (NBIS), among the various operating condition stability evaluations, the  $\Delta$  threshold voltage ( $V_{th}$ ) of the IGZO (Ga: 3%) TFT ( $-7.6$  V) was 23% better than that of the IZO TFT ( $-9.8$  V); however,  $\Delta V_{th}$  of the IYZO (Yb: 3%) ( $-5.8$  V) TFT was not only 41% better than that of the IZO TFT but also 19% better than that of the IGZO TFT. Under NBIS conditions, the deep level oxygen vacancy ( $V_O$ ) donates electrons to the conduction band minimum, causing a large negative shift in  $V_{th}$ . Therefore, the improved stability of the IYZO TFT indicates that Yb doping effectively reduced the formation of defect state like deep level  $V_O$ , which was demonstrated by theoretical density functional calculations. In addition, the mobility of the IYZO TFT was  $12.22\text{ cm}^2\text{ V}^{-1}\text{ s}^{-1}$ , which was 3% better than that of the IZO TFT ( $11.83\text{ cm}^2\text{ V}^{-1}\text{ s}^{-1}$ ). Conversely, the mobility of the IGZO TFT was  $10.34\text{ cm}^2\text{ V}^{-1}\text{ s}^{-1}$ , demonstrating a 13% decrease compared to the IZO TFT. Notably, Ga doping improved the stability but degraded the electrical performance, whereas Yb doping improved the stability and electrical properties.

Received 26th December 2024,  
Accepted 30th May 2025

DOI: 10.1039/d4tc05455e

rsc.li/materials-c

## 1. Introduction

Oxide thin-film transistors (TFTs) based on amorphous oxide semiconductors (AOSs) are applied to ultra-high resolution and high-definition displays owing to their excellent carrier mobility, low off-current, and good transmittance in the visible region.<sup>1,2</sup> Oxide TFTs are fabricated by vacuum processes such as sputtering<sup>3,4</sup> and atomic layer deposition,<sup>5,6</sup> as well as by solution processes such as spin coating<sup>7,8</sup> and ink-jet printing.<sup>9,10</sup> Vacuum-processed oxide TFTs minimize contamination from residual gas

because they require base pressures in the high-vacuum range. This results in negligible defects and good uniformity of the films, leading to excellent electrical performance and stability of the TFTs. However, the process is costly and is difficult to apply to large area displays.<sup>11</sup> In contrast, solution-processed oxide TFTs are gaining attention owing to their advantages such as a simple process, low cost, excellent composition control, and suitability for large application area displays.<sup>12</sup> However, because the quality of the film is poor owing to defects formed due to impurities, such as metal-hydroxyl groups (M-OH) and carbon, the mobility and subthreshold swing are reduced, thereby decreasing the electrical properties.<sup>13</sup> In particular, the degradation of stability characteristics under various operating conditions such as the gate, illumination, and thermal bias stress is a major obstacle for commercialization. Therefore, to overcome the problem of stability of solution-processed oxide TFTs, various studies have been conducted considering the device structure, annealing process, and introduction of new compositions of channel materials.

Regarding the device structure, research has focused on improving the stability of TFTs by applying a top gate structure, which protects the channel area from external environments including illumination and acts as a light shield to improve the

<sup>a</sup> Nano Convergence Materials Center, Korea Institute of Ceramic Engineering and Technology (KICET), Jinju 52851, Republic of Korea. E-mail: laser02hj@kicet.re.kr, soowon.heo@kicet.re.kr

<sup>b</sup> Department of Electrical and Electronics Engineering, Pusan National University, Busan 46241, Republic of Korea. E-mail: msyi@pusan.ac.kr

<sup>c</sup> Division of Materials Science and Engineering, Hanyang University, Seoul 04763, Republic of Korea

<sup>d</sup> Department of Materials Science and Engineering, Ajou University, Suwon 16499, Republic of Korea

<sup>e</sup> Department of Energy Systems Research, Ajou University, Suwon 16499, Republic of Korea

† Electronic supplementary information (ESI) available. See DOI: <https://doi.org/10.1039/d4tc05455e>

characteristics under these conditions. However, it is difficult to commercialize because the existing Si-based process line cannot be applied.<sup>14,15</sup>

Several studies regarding stability improvement *via* annealing have also been conducted. Processes such as deep ultraviolet-thermal dual treatment<sup>16,17</sup> and plasma treatment<sup>18</sup> promote the formation of metal–oxygen–metal networks owing to reactive oxygen, thereby reducing the defects in the film and contributing to improved stability. However, oxide TFTs, which are compounds consisting of an ionic bond between a metal cation and an oxide anion, require high energy for the annealing process and have a narrow process window because they can only absorb part of the UV region owing to their high bandgap of greater than 3 eV.

Finally, several studies have been conducted to develop new compositions of channel materials to improve the stability of oxide TFTs. The compositions of these materials include indium–zinc oxide (IZO),<sup>19</sup> indium–zinc–tin oxide (IZTO),<sup>20</sup> indium–gallium–tin oxide (IGTO),<sup>21</sup> indium–gallium–zinc–tin oxide (IGZTO),<sup>16,22</sup> and zinc–tin oxide (ZTO),<sup>23</sup> as well as materials that have been developed by doping elements to apply to TFTs. The conditions were optimized by varying the molar ratios of elements with high metal–oxygen binding energies in the composition of materials such as IZO, IZTO, and IGZTO, thereby effectively suppressing the oxygen vacancies ( $V_O$ ) to improve stability. However, many studies have been conducted on varying molar ratios, which limits the search for new compositions. Notably, ions with a high oxygen dissociation energy, such as zirconium,<sup>24</sup> boron,<sup>25</sup> terbium (Tb),<sup>26</sup> or yttrium,<sup>27</sup> reduce the defects at the interface of the gate insulator and active layer *via* doping, which inhibits the trapping of carriers and effectively improves the stability. However, a high doping content can induce both  $V_O$  suppression and charge trapping, leading to an adverse effect on the stability.<sup>13,28</sup>

IZO TFTs, which are one of the leading oxide semiconductors, have been significantly studied owing to their high electrical mobility, but they demonstrate poor reliability and stability when subjected to bias stress tests.<sup>29</sup> In particular, subgap defects on the back channel surface are photoexcited under an illumination bias stress, resulting in the trapping of delocalized electrons within the conduction band minimum (CBM). This causes the threshold voltage ( $V_{th}$ ) of oxide TFTs to significantly shift to the negative direction, resulting in instability.<sup>30</sup> Socratous *et al.* studied the improvement of the electrical performance and stability of solution processed IZO TFTs through the annealing process.<sup>31</sup> As the annealing temperature increased, certain oxygen defects formed a shallow donor level near the CBM rather than the deep state near the valence band minimum (VBM). A shallow donor level is related to the carrier concentration, which can be attributed to the increased mobility. Furthermore, a reduction in hysteresis was derived from the decreased amount of trap sites within the band gap. However, for high-temperature annealing above 400 °C, the large increase in the carrier concentration can cause a negative shift in  $V_{th}$ , which can worsen the stability.<sup>32</sup> Therefore, the optimization of research that effectively reduces trapping while minimizing the degradation of the electrical

performance is essential. Liu *et al.* investigated the effect of Tb doping on the bias stability of IZO TFTs.<sup>26</sup> This caused the electron–holes of  $Tb^{3+}$  and  $Vn + O$  to recombine, reducing the trapping of positive charges, which was effective in reducing  $\Delta V_{th}$  under a negative bias illumination stress (NBIS). However, as the dopant concentration increased, the electrical performance degraded. Most of the previously reported studies regarding the increase in device stability demonstrate a decrease in carrier mobility owing to a decrease in  $V_O$ , which degrades the transport properties.<sup>24–27</sup> Therefore, the trade-off between mobility and stability must be overcome for the active commercialization of oxide TFTs.

Gallium (Ga) is a typical dopant used for improving the electrical properties and stability of IZO TFTs. It has a high metal–oxide dissociation energy of 285 kJ mol<sup>-1</sup> and an ionic radius similar to In and Zn, which can effectively reduce  $V_O$  to increase the stability and reduce the generation of electron traps in the compound.<sup>33</sup> However, the cost of Ga significantly fluctuates, and it is difficult to obtain a stable supply. Therefore, there is an increasing need for research to introduce new materials that can reduce or replace Ga.

Ytterbium (Yb) is the most abundant rare earth element with a standard electrode potential of -2.19 V that is significantly lower than that of indium (In) (0.34 V) and zinc (Zn) (-0.76 V). In addition, its electronegativity is 1.1, which is also lower than that of In (1.78) and Zn (1.65). The metal–oxide dissociation energy of Yb–O is 397.9 kJ mol<sup>-1</sup>, which is higher than that of In–O (360 kJ mol<sup>-1</sup>) and Zn–O (284.1 kJ mol<sup>-1</sup>);<sup>34,35</sup> in particular, since it is higher than that of Ga (285 kJ mol<sup>-1</sup>),  $V_O$ , which is a larger source of instability in oxide TFTs, can be effectively reduced compared to Ga. Xu *et al.* investigated the effect of Yb doping on the bias stability of  $InO_3$  TFTs.<sup>35</sup> The incorporation of Yb was found to promote the formation of the oxide lattice, significantly reducing the off current. However, the optimized In–Yb–O film with the Yb concentration of 10% exhibited a low mobility of 8 cm<sup>2</sup> V<sup>-1</sup> s<sup>-1</sup> and showed considerable threshold voltage shifts of approximately -10 V and -11 V under negative and positive bias stress (NBS and PBS), respectively. These degradations in electrical performance are attributed to the incomplete dehydration of residual  $Yb(OH)_3$  due to excessive doping. Therefore, optimizing dopant concentration is essential to achieve stable device performance.

This study aims to propose a new composition of indium–ytterbium–zinc oxide (IYZO), where IZO is doped with Yb. Using IZO (In : Zn = 1 : 1) with an excellent electrical performance as the criterion channel, an indium–gallium–zinc oxide (IGZO) TFT doped with Ga was also fabricated to compare the effect of Yb on the electrical properties of the TFTs. Ga and Yb were doped at 1, 3, and 5% and optimized at 3% each. The IYZO (Yb: 3%) TFT was evaluated for a bias stress under various conditions including NBS, PBS, NBIS, negative bias illumination stress (NBTS), and positive bias stress (PBTS);  $\Delta V_{th}$  was reduced by 20%, 24%, 24%, 44%, and 44%, respectively, compared to IGZO (Ga: 3%) TFTs. These results indicate that IYZO TFTs effectively reduce the instability-causing  $V_O$  more than IGZO TFTs, and density functional theory (DFT) calculations

demonstrate that IYZO films have a higher deep V<sub>O</sub> formation energy than IGZO films. Notably, the mobility of the IGZO TFT decreased by 13% to  $10.34 \text{ cm}^2 \text{ V}^{-1} \text{ s}^{-1}$  compared to that of the IZO TFT ( $11.83 \text{ cm}^2 \text{ V}^{-1} \text{ s}^{-1}$ ), whereas that of the IYZO TFT increased to  $12.22 \text{ cm}^2 \text{ V}^{-1} \text{ s}^{-1}$ . As a result, a new composition of the oxide TFT that improves the stability and electrical mobility was proposed.

## 2. Experimental

### 2.1. Synthesis of metal oxide solutions

The IZO solution was synthesized by dissolving 0.1 M indium chloride and 0.1 M zinc acetate dihydrate in 2-methoxy ethanol. In addition, 1% to 5% of ytterbium chloride hexahydrate and gallium nitrate were added to the IZO solution for dissolving, respectively, to synthesize a total of seven solutions. After dissolving the metal precursor in the solvent, the solution was stirred at 80 °C and 700 rpm for 4 h.

### 2.2. Metal oxide layer deposition and device fabrication

The gate insulator and gate were used as SiO<sub>2</sub>/Si wafers with a 100 nm SiO<sub>2</sub> layer grown by wet oxidation on heavily doped silicon (P+Si), respectively. Prior to coating the active layer, the SiO<sub>2</sub>/Si wafer was cleaned in an ultrasonic cleaner using several solutions in the following order: deionized (D.I.) water, acetone, methanol, isopropyl alcohol, and D.I. water for 10 min each, after which it was dried on a 150 °C hotplate for 10 min. The SiO<sub>2</sub>/Si wafers were irradiated for 10 min in an ultra-violet ozone cleaner (AC-16, AhTech) to remove the organic residue on the SiO<sub>2</sub>/Si wafers and improve adhesion. For the IZO, IYZO, and IGZO thin films, each solution was spin coated onto the SiO<sub>2</sub>/Si substrate at 5000 rpm for 20 s and pre-annealed on a hotplate at 150 °C for 10 min to dry the solvent. All the devices were thermally annealed at 550 °C for 1 h in an electric furnace in ambient air, and the channels of the device were patterned with the hydrogen chloride etchant. The ITO source/drain was deposited at 100 nm by magnetron sputtering and patterned *via* a lift-off process to define the width and length of the active channel at 100 and 80 μm, respectively. Fig. 1(a) shows a

schematic illustration of the IYZO TFT, and Fig. 1(b) presents a high-resolution cross-sectional TEM image. Based on the TEM analysis, the thickness of the active layer was confirmed to be approximately 12 nm ( $\pm 1$  nm). Furthermore, no significant thickness variation was observed among the films, regardless of the Yb and Ga concentrations.

### 2.3. Computational details

DFT calculations were performed with the Vienna Ab initio Simulation Package<sup>36,37</sup> (VASP) using the projector augmented-wave method with generalized gradient approximation (GGA) within the Perdew–Burke–Ernzerhof (PBE) framework.<sup>38,39</sup> The plane-wave basis set was expanded to a cutoff energy of 520 eV to minimize Pulay stress during structural optimization. The structural optimization was truncated until the Hellmann–Feynman forces were under  $0.01 \text{ eV } \text{\AA}^{-1}$ . Electronic energy convergence was set to  $1 \times 10^{-5} \text{ eV}$ . The Brillouin zone was sampled using 100 *k*-points density per inverse Å<sup>3</sup> of the reciprocal cell. To achieve a more accurate calculation of the electronic structure than the PBE-GGA functional, the meta-GGA functional was employed with the modified Becke–Johnson (MBJ) potential.<sup>40,41</sup> To model the amorphous IZO, *ab initio* molecular dynamics (AIMD) simulations were performed using Crystal Hamiltonian Graph neural Network (CHGNet) packages.<sup>42</sup> The initial atomic structure of amorphous IZO was modeled with 30 indium, 30 zinc, and 75 oxygen atoms with a density of 6.108 g cm<sup>-3</sup>. Subsequently, amorphous structures were melted for 5 ps at 2500 K and then cooled down to 300 K at a rate of 200 K ps<sup>-1</sup>. The formation energy of an oxygen vacancy was calculated as follows:

$$\Delta E^f(V_O) = E_{\text{defective system}} - E_{\text{perfect system}} + n_i 1/2 \mu_{O_2} \quad (1)$$

where  $E_{\text{defective system}}$  is the total energy of the supercell containing an oxygen vacancy,  $E_{\text{perfect system}}$  is the total energy of the pristine supercell,  $n_i$  is the number of oxygen vacancies, and  $\mu_{O_2}$  is the chemical potential of oxygen. Since we focus on a single oxygen vacancy in our calculations, we set  $n_i = 1$ . In this work, we consider  $\mu_{O_2} = \frac{1}{2}E(O_2)$  where  $E(O_2)$  is the total energy of O<sub>2</sub> in the gas phase.

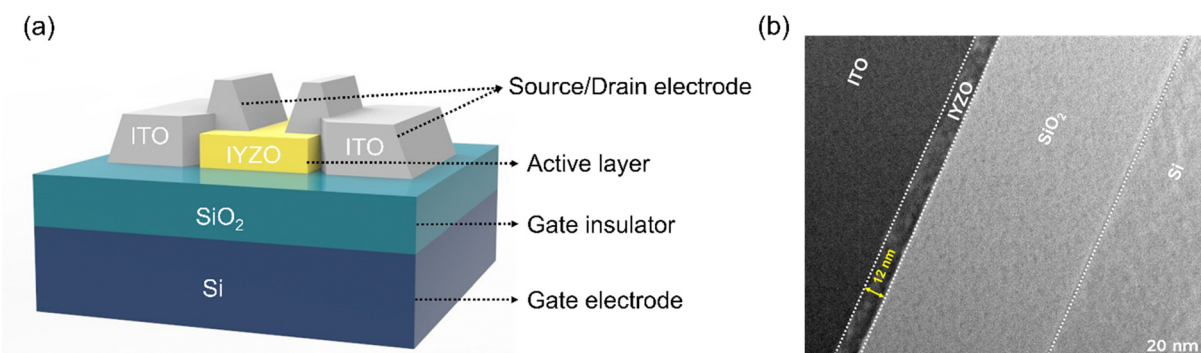


Fig. 1 (a) Schematic illustration of the top-contact bottom-gate IYZO TFT. (b) Cross-sectional HR-TEM images of the IYZO TFT.

#### 2.4. Electrical and material characterization

The cross-sectional image of the IYZO TFT was measured using transmission electron microscopy (TEM) (JEM-4010, Jeol). The electrical properties and bias stress tests of the devices were measured in ambient air and using an HP 4145B semiconductor parameter analyzer (Hewlett Packard). The transfer curve was measured by sweeping the gate voltage range from  $-40$  to  $40$  V in  $0.2$  V steps. The surface roughness was measured using an atomic force microscope (AFM) (NX20 300 nm, Park Systems). IZO, IYZO, and IGZO thin films for the analysis of carrier concentration, Hall mobility, and resistivity were fabricated through a repeated spin-coating process and analyzed at room temperature using a hall measurement system (HMS-5000, Ecopia). The chemical compositions of the IZO, IYZO, and IGZO thin films were analyzed using an X-ray photoelectron spectrometer (XPS) (Al K $\alpha$  (1486.68 eV) NEXSA XPS, Thermo Fisher Scientific), and the binding energy was calibrated to  $284.7$  eV using the C 1s peak. The optical bandgap energies of the IZO, IYZO, and IGZO films were measured by UV-visible spectroscopy (V-670, Jasco) and were Tauc-plotted. The crystalline structures of the IZO, IYZO, and IGZO thin films were analyzed using a grazing incidence X-ray diffraction (GI-XRD) (D8 Advance A25 Plus, Bruker).

### 3. Results and discussion

Fig. 2(a) and (b) and Fig. S1 (ESI $\dagger$ ) demonstrate the transfer characteristics and the output characteristics, respectively, to compare the electrical characteristics of the IZO, IGZO, and IYZO TFTs, which are summarized in Table 1. Fig. 2(a) demonstrates that as the Ga content increased from  $0\%$  to  $5\%$ , the value of  $V_{th}$  shifted to positive and the on-current decreased. Fig. 2(b) demonstrates that similar to Ga doping, a higher Yb content shifted the value of  $V_{th}$  to be positive. This indicates that the incorporation of Yb/Ga effectively reduces the carrier concentration in IZO, functioning as an electronic de-doping mechanism. In contrast, the on-current increased at a Yb doping concentration of  $1\%$  doping and then decreased at  $3\%$  and  $5\%$ . Notably, the on current of the IYZO TFT was lower than that of the IYZO (Yb:  $1\%$ ) TFT, but it showed a higher on current than the IZO TFT. The decrease in the on-current with the doping of Ga and Yb is a result of the strong binding of the dopants to oxygen, resulting in a decrease in  $V_o$  because mobility is strongly dependent on the electron concentration generated by  $V_o$ . However, the IYZO TFTs demonstrated a smaller decrease in the on-current. Fig. S2 (ESI $\dagger$ ) shows the full characteristics for a gate voltage sweep from  $-40$  C to  $40$  V. It can be observed that the transfer between the trace and retrace curve exhibits a negligible shift. Fig. 2(c) and (d) present the hall mobility and carrier concentration according to the hall measurement of the IZO, IYZO, and IGZO films with different doping concentrations. The carrier concentration decreased to  $1.26 \times 10^{16}$  cm $^{-3}$  for the IGZO film and  $1.26 \times 10^{16}$  cm $^{-3}$  for the IYZO film compared to  $1.48 \times 10^{16}$  cm $^{-3}$  for the IZO film, and gradually decreased as the Ga or Yb doping concentration

increased. Therefore, the doping of Yb or Ga reduced the carrier concentration, thereby increasing the resistance of the channel layer. The difference between Hall mobility and field-effect mobility is likely attributed to interfacial charge scattering or degraded charge transport caused by the formation of multi-layered structures, as reported in a previous study.<sup>24</sup>

The decrease in the hall mobility as the doping concentration increased was similar to the mobility trend of IZO, IGZO, and IYZO TFTs, as shown in Fig. 2(e), which is consistent with previous studies.<sup>43,44</sup> Because the dissociation energies of Yb-O ( $397.9$  kJ mol $^{-1}$ ) and Ga-O ( $285$  kJ mol $^{-1}$ ) are higher than those of In-O and Zn-O,  $V_o$  can be suppressed via doping.  $V_o$  provides electrons to increase the carrier concentration, while it causes instability. The decrease in the hall mobility is attributed to the decrease in  $V_o$  as the doping concentration increases; these results are consistent with the decrease in mobility and the on/off current as the Ga and Yb doping concentration increases, as shown in Fig. 2(a) and (b). Fig. 2(e) demonstrates the doping concentration-dependent mobility of the IZO, IGZO, and IYZO TFTs. The mobility was

$$\text{obtained by the following equation: } \mu_{lin} = \frac{L}{WC_{ox}V_D} \left( \frac{\delta I_D}{\delta V_G} \right).$$

A total of  $10$  TFTs were fabricated for each condition, for which the average values are shown; the deviation is shown in Fig. S3 (ESI $\dagger$ ).  $C_{ox}$  is the oxide capacitance per unit area,  $L$  and  $W$  are the channel length and width, respectively. The mobility of the IGZO TFTs decreased as the ratio of Ga increased in the IZO TFTs ( $11.83$  cm $^2$  V $^{-1}$  s $^{-1}$ ), demonstrating a  $19\%$  decrease to  $9.61$  cm $^2$  V $^{-1}$  s $^{-1}$  for the IGZO (Ga:  $5\%$ ) TFTs. However, the mobility of the IYZO (Yb:  $1\%$ ) TFTs demonstrated an  $8\%$  improvement to  $12.81$  cm $^2$  V $^{-1}$  s $^{-1}$  compared to the IZO TFTs, whereas the IYZO and IYZO (Yb:  $5\%$ ) TFTs demonstrated a smaller decrease to  $12.22$  cm $^2$  V $^{-1}$  s $^{-1}$  and  $10.88$  cm $^2$  V $^{-1}$  s $^{-1}$ , respectively. It could be predicted owing to the result that Yb doping reduces the scattering of electrons from defects between the channel layer and gate insulator layer owing to the reduction of impurities by promoting M-O bonding because Yb (1.1) has a lower electronegativity than Ga (1.81) because this electron scattering at the interface can contribute to a decrease in mobility by interfering with the transport path of electrons. The cause of increase in the electrical performance of IYZO (Yb:  $1\%$ ) in Fig. 2(b), (d), and (e) is discussed later in the section presenting the band edge state analysis.

Table 1 presents the electrical characteristics of the IZO, IGZO, and IYZO TFTs fabricated with different doping ratios. The  $V_{th}$  was determined by the value of gate bias ( $V_{GS}$ ), which induced a drain current ( $I_{DS}$ ) of  $L/W \times 10^{-8}$  A at a drain bias ( $V_{DS}$ ) of  $1.1$  V. The subthreshold swing (SS) was obtained by the following equation:

$$SS = \left( \frac{d \log(I_{DS})}{d V_{GS}} \right)^{-1} \quad (2)$$

where  $I_{DS}$  denotes the drain-source current. To investigate the influence of the trap state on the electrical property, the interface trap density ( $D_{it}$ ) of the channel/gate insulator was

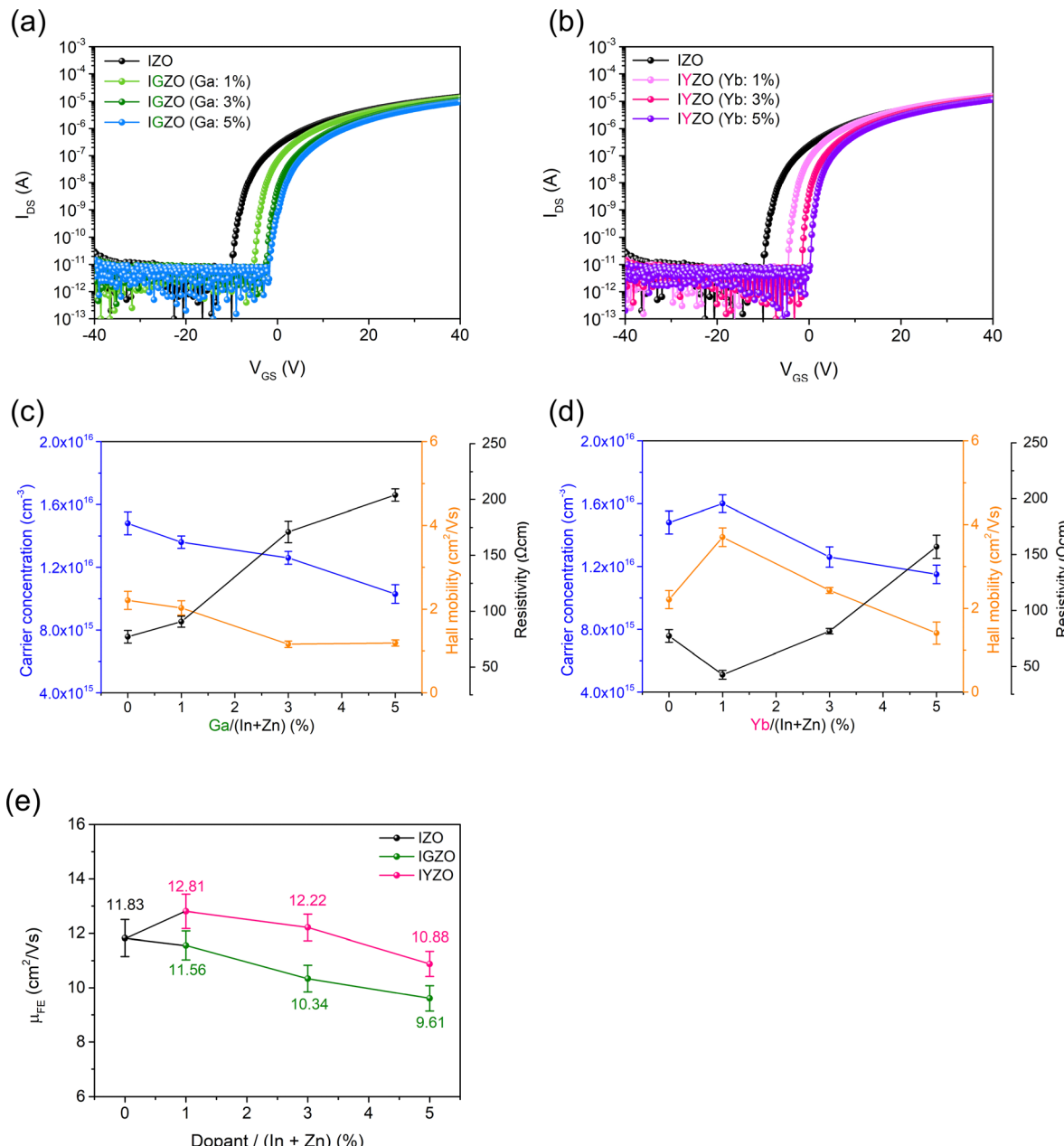


**Fig. 2** Transfer characteristics of (a) IZO TFTs and IGZO TFTs with various (1, 3, and 5%) Ga concentrations and (b) IZO TFTs and IYZO TFTs with various (1, 3, and 5%) Yb concentrations. Hall measurement characteristics of IZO TFTs with (c) various Ga concentrations and (d) various Yb concentrations. (e) Mobility of IZO TFTs and IGZO, IYZO TFTs fabricated with various dopant (Ga/Yb) ratios. The average and standard deviation values of hall measurement characteristics and field effect mobility were extracted from 10 devices.

**Table 1** Electrical parameters of the IZO, IGZO, and IYZO TFTs with various dopant (Ga/Yb) ratios. The average and standard deviation values were extracted from 10 devices

	Mobility ( $\text{cm}^2 \text{V}^{-1} \text{s}^{-1}$ )	$V_{th}$ (V)	SS (V decade $^{-1}$ )	$D_{it} (\times 10^{12}, \text{cm}^{-2} \text{eV}^{-1})$	On/off ratio ( $\times 10^6$ )
IZO	$11.83 \pm 0.68$	$-6.58 \pm 0.86$	$1.36 \pm 0.21$	$4.85 \pm 0.80$	$2.73 \pm 1.00$
IGZO	$11.56 \pm 0.53$	$-2.58 \pm 1.09$	$1.17 \pm 0.20$	$4.17 \pm 0.76$	$2.66 \pm 0.18$
	$10.34 \pm 0.49$	$0.2 \pm 0.49$	$0.90 \pm 0.13$	$3.15 \pm 0.48$	$2.28 \pm 0.15$
	$9.61 \pm 0.47$	$1.96 \pm 0.49$	$1.03 \pm 0.14$	$3.61 \pm 0.53$	$2.04 \pm 0.13$
IYZO	$12.81 \pm 0.40$	$-2.46 \pm 0.49$	$0.95 \pm 0.18$	$3.34 \pm 0.69$	$3.16 \pm 0.12$
	$12.22 \pm 0.49$	$-0.02 \pm 0.49$	$0.68 \pm 0.11$	$2.34 \pm 0.42$	$3.04 \pm 0.14$
	$10.88 \pm 0.46$	$1.76 \pm 0.49$	$0.71 \pm 0.09$	$2.40 \pm 0.35$	$2.39 \pm 0.13$

calculated with the following equation using the SS value obtained:

$$D_{it} = \frac{C_{ox}}{q} \left( \frac{qSS}{kT \ln 10} - 1 \right) \quad (3)$$

where  $q$  denotes the charge of an electron,  $k$  denotes the Boltzmann constant, and  $T$  denotes the absolute temperature. Compared to the IZO TFTs, the SS values of the IGZO and IYZO TFTs decreased from  $1.36 \text{ V decade}^{-1}$  to  $0.90 \text{ V decade}^{-1}$  and  $0.68 \text{ V decade}^{-1}$ , respectively. As a result, the value of  $D_{it}$  was as high as  $4.85 \text{ cm}^{-2} e^{-1} \text{ V}^{-1}$  for the IZO TFTs but significantly decreased to  $3.15 \text{ cm}^{-2} e^{-1} \text{ V}^{-1}$  for the IGZO TFTs and  $2.34 \text{ cm}^{-2} e^{-1} \text{ V}^{-1}$  for the IYZO TFTs. These effects indicate that Ga and Yb doping reduce the defects at the channel layer and gate insulator layer interface of the IZO TFT, leading to a reduction in the amount of trap states, consequently reducing the carrier trapping defects and thus improving the switching characteristics. Furthermore, Ga and Yb doping improved the quality of the channel/gate insulator interface and channel layer, as reported in previous studies.<sup>28,45</sup> In particular, the SS value of the IYZO TFT was reduced by 53% and the  $D_{it}$  value was reduced by 56% compared to the IZO TFTs, confirming that the defects were effectively reduced compared to the IGZO TFTs. The reductions in SS and  $D_{it}$  are attributed to the decrease in oxygen-related trap states, such as  $V_O$ , which is discussed in the subsequent XPS analysis.

Fig. 3 presents the bias stress stability test results of the IZO, IGZO, and IYZO TFTs at  $V_{GS} = \pm 10 \text{ V}$  and  $V_{DS} = 1.1 \text{ V}$ . The illumination stress was set to 1000 lux for the light source and temperature stress was set to  $60^\circ\text{C}$ . Fig. 3(a)–(c) shows PBS, Fig. 3(d)–(f) shows NBS, Fig. 3(g)–(i) shows PBTS, Fig. 3(j)–(l) shows NBTS, Fig. 3(m)–(o) shows PBIS, and Fig. 3(p)–(r) shows  $\Delta V_{th}$  values under NBIS, which are summarized in Fig. 3(s) and Table 2. The values of  $\Delta V_{th}$  under the PBS and NBS conditions of the IZO TFT were  $5.6 \text{ V}$  and  $-5.4 \text{ V}$ , respectively (Fig. 3(a) and (d)). The  $\Delta V_{th}$  values of the IGZO TFT under the PBS and NBS conditions decreased by 40% and 26% to  $+3.4 \text{ V}$  and  $-4 \text{ V}$ , respectively (Fig. 3(b) and (e)). Conversely, the IYZO TFT demonstrated a relatively good stability with  $\Delta V_{th}$  values of  $+2.6 \text{ V}$  and  $-3.2 \text{ V}$  under PBS and NBS conditions, respectively, indicating a decrease of 54% and 41% compared to the IZO TFT (Fig. 3(c) and (f)). Impurities, such as those owing to  $V_O$  and M-OH, are typical factors that act as defects in the film, forming electron/hole trap sites and causing instability. Therefore, the comparatively better bias stability of the IYZO TFTs compared to that of the IGZO TFT was likely due to the higher dissociation energy of Yb-O ( $397.9 \text{ kJ mol}^{-1}$ ) compared to that of Ga-O ( $285 \text{ kJ mol}^{-1}$ ), which effectively reduced  $V_O$ . In a previously reported In-Yb-O TFT, a significant  $\Delta V_{th}$  exceeding  $\pm 10 \text{ V}$  was observed under both NBS and PBS conditions, despite the incorporation of 10% Yb.<sup>35</sup> This instability was attributed to charge trapping caused by excessive Yb doping, which had been introduced to suppress the high density of  $V_O$  in  $\text{In}_2\text{O}_3$ . In contrast, in this study, improved stability was achieved due to a reduced density of interface defect states at the IYZO/SiO<sub>2</sub> interface, which is consistent with the observed

decrease in trap density. The stability under the PBTS and NBTS conditions was also evaluated (Fig. 3(m)–(r)). As a result, the  $\Delta V_{th}$  value of the IZO TFTs under the PBTS and NBTS conditions was found to be  $+6.8 \text{ V}$  and  $-8.2 \text{ V}$ , respectively. The IGZO TFT demonstrated a 27% and 27% decrease to  $+5 \text{ V}$  and  $-6 \text{ V}$ , respectively, compared to those of the IZO TFT, whereas the IYZO TFT demonstrated a significant decrease of 59% and 59% to  $+2.8 \text{ V}$  and  $-3.4 \text{ V}$ , respectively. Thermal induced holes from defect states are accumulated by the negative gate voltage and trapped at the interface. As a result, the  $V_{th}$  value causes a large shift in the negative direction. The excellent stability of the IYZO TFT under temperature bias stress is attributed to Yb doping, which not only reduces  $V_O$  and suppresses the generation of thermally excited electrons but also effectively decreases interface defects.<sup>46</sup> Fig. 3(g)–(l) present the stability evaluation results under the PBIS and NBIS conditions. Under the PBIS condition, the  $\Delta V_{th}$  value of the IZO TFTs was  $+4.8 \text{ V}$ , whereas that of the IGZO TFT was reduced by 55% to  $+2.2 \text{ V}$ , and that of the IYZO TFT was reduced by 75% to  $+1.2 \text{ V}$ . Notably, under the NBIS condition, compared to the IZO TFT with a  $\Delta V_{th}$  of  $-9.8 \text{ V}$ , the IGZO TFT ( $-7.6 \text{ V}$ ) demonstrated a 23% decrease, but the IYZO TFT ( $-5.8 \text{ V}$ ) demonstrated excellent photo-bias stability with a 41% decrease. Among  $V_O$  defects, deep-level  $V_O$  creates defect states between forbidden bandgaps, causing bias instability, especially severe negative shifts in  $V_{th}$  under the NBIS.<sup>30</sup> Therefore, the excellent bias stability of the IYZO TFT under illumination is due to the suppression of formation of deep-level  $V_O$ . This suggests that Yb is a dopant for the IZO TFT that effectively reduces the defects that cause instability.

Bias and illumination stress are caused by trapping at interface defect states and the contribution of free electrons from photoexcitation at subgap defect states. Notably, under illumination stress, instability induced by photoexcitation of deep-level  $V_O$  is dominant.<sup>47</sup> Fig. 4 presents the analysis of the photo-response characteristics to evaluate the electrical performance of the IZO, IGZO, and IYZO TFTs under illumination without bias stress, which was fixed at 500 lux. Fig. 4(a) demonstrates that for the IZO TFT, the value of  $\Delta V_{th}$  was negatively shifted to  $-2.6 \text{ V}$  under illumination which was due to the deep-level  $V_O$  near the VBM being excited to  $V_O^{2+}$  by the illumination and donating electrons to the conduction band, consequently resulting in a large negative shift of the transfer curve.<sup>30,43</sup> Conversely, the photo-response characteristic was suppressed for the IYZO TFT and IGZO TFT as shown in Fig. 4(b) and (c), indicating that Ga and Yb doping play an important role in mitigating the photo-response instability of TFTs by reducing the instability-causing  $V_O$ . In particular, the IGZO TFT has a  $\Delta V_{th}$  of  $-1.4 \text{ V}$ , whereas that value for the IYZO TFT is  $-1 \text{ V}$ , which is a 29% reduction. This indicates that Yb doping effectively reduces deep-level  $V_O$  more than Ga. Fig. S4 (ESI†) presents the photoresponse characteristics of the IGZO (Ga: 1%), (Ga: 5%), and IYZO (Yb: 1%), (Yb: 5%) TFTs, demonstrating that  $\Delta V_{th}$  decreased as the concentration of Ga or Yb increased. These results indicate that  $V_O$  decreases as the doping concentration of Ga and Yb increases. In particular, the IYZO film was demonstrated by good photo response

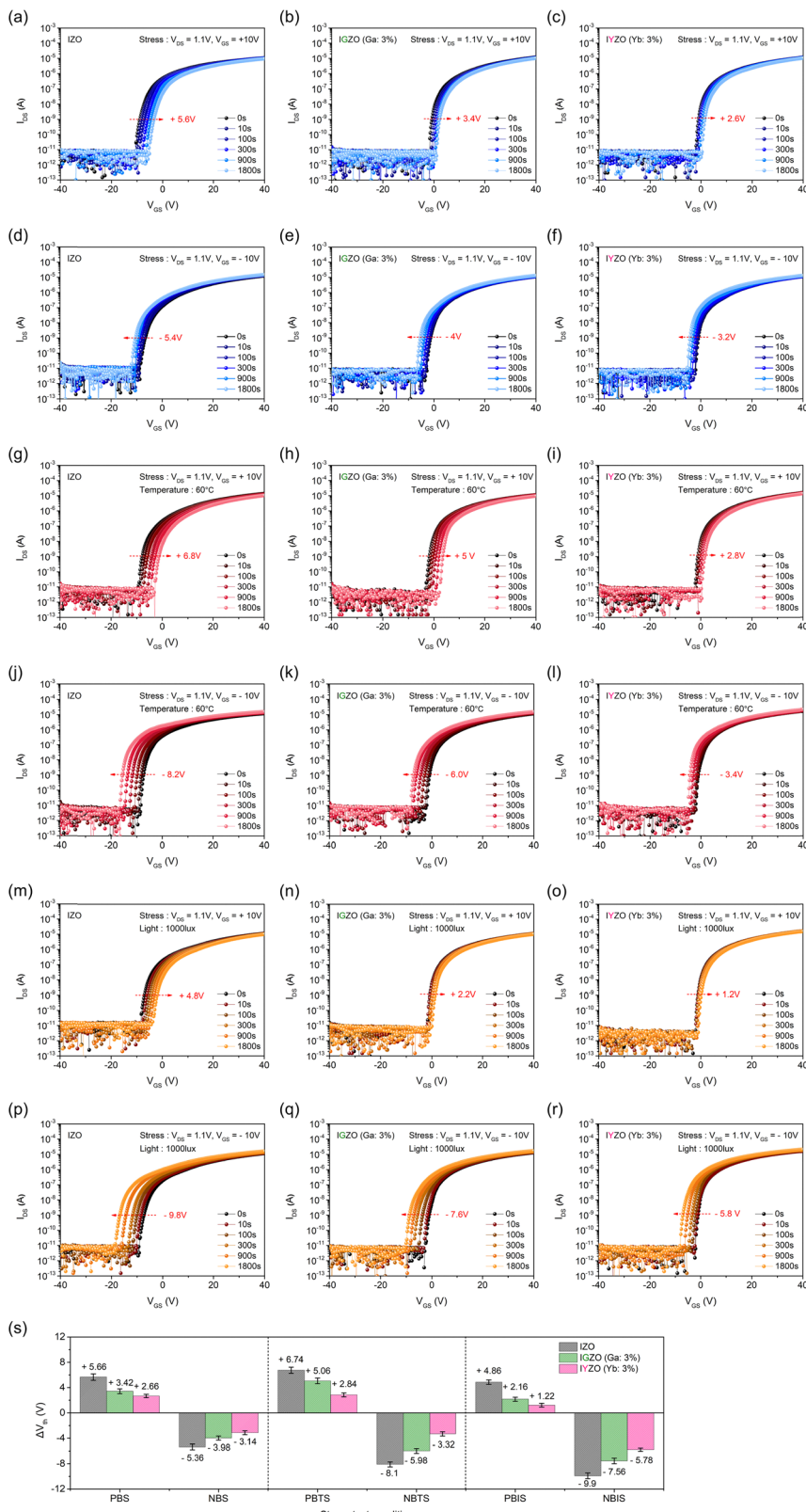


**Fig. 3** (a)–(c) Positive bias stress, (d)–(f) negative bias stress, (g)–(i) positive bias illumination stress, (j)–(l) negative bias illumination stress, (m)–(o) positive bias temperature stress, and (p)–(r) negative bias temperature stress test for the IZO TFT, IGZO (Ga: 3%) TFT, and IYZO (Yb: 3%) TFT, respectively. (s) Threshold voltage shift ( $\Delta V_{th}$ ) of the IZO TFT, IGZO (Ga: 3%) TFT, and IYZO (Yb: 3%) TFTs under various stress conditions. Average and standard deviation extracted from 10 devices.

**Table 2** Threshold voltage shifts ( $\Delta V_{th}$ ) of the IZO, IGZO (Ga: 3%), and IYZO (Yb: 3%) TFTs under various stress conditions. Average and standard deviation extracted from 10 devices

	$\Delta V_{th}$ of TFTs under various stress test conditions [V]					
	PBS	NBS	PBTS	NBTS	PBIS	NBIS
IZO	+5.66 ± 0.50	-5.36 ± 0.44	+6.74 ± 0.49	-8.10 ± 0.39	+4.86 ± 0.35	-9.90 ± 0.45
IGZO (Ga: 3%)	+3.42 ± 0.38	-3.98 ± 0.32	+5.06 ± 0.43	-5.98 ± 0.38	+2.16 ± 0.31	-7.56 ± 0.44
IYZO (Yb: 3%)	+2.66 ± 0.27	-3.14 ± 0.31	+2.84 ± 0.31	-3.32 ± 0.34	+1.22 ± 0.30	-5.78 ± 0.27

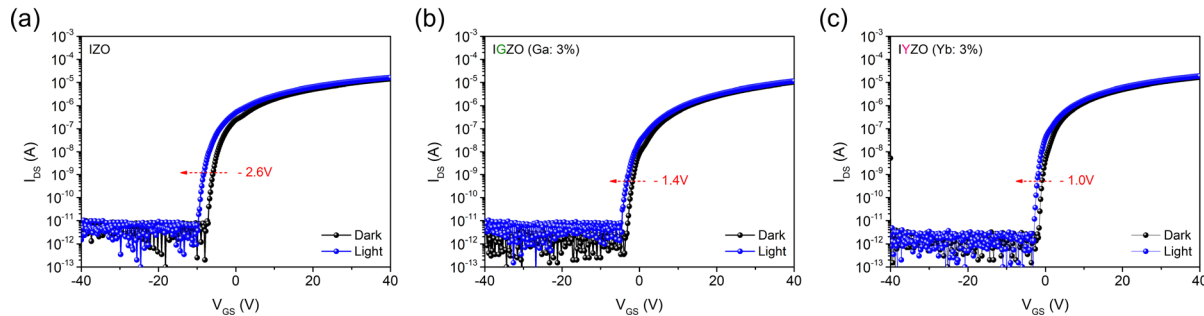


Fig. 4 Photo-response of the (a) IZO TFT, (b) IGZO (Ga: 3%) TFT, and (c) IYZO (Yb: 3%) TFT, respectively.

suppression, confirming that Yb doping is more effective than Ga in reducing the formation of subgap defect states and improving the negative shift due to illumination.

The XPS analysis confirmed the effect of Ga and Yb doping on the electrical characteristics and stability of TFTs. Fig. 5 presents the O 1s spectra of IZO, IGZO (Ga: 3%), and IYZO (Yb: 1, 3, and 5%), respectively. The O 1s spectrum was analyzed using Gaussian fitting and separated into metal–oxygen (M–O) bonding (529.8 eV ± 0.05), VO (531.1 eV ± 0.05), and impurities such as OH<sup>−</sup> bonding (532.1 eV ± 0.05) peaks,<sup>21</sup> which were

labeled as O<sub>I</sub>, O<sub>II</sub>, and O<sub>III</sub>, respectively. For the IZO film shown in Fig. 5(a), the percentages of O<sub>I</sub>, O<sub>II</sub>, and O<sub>III</sub> were calculated to be 53.69%, 44.67%, and 1.64%, respectively. The O<sub>II</sub> ratio of the IGZO film shown in Fig. 5(b) was 32.51%, which demonstrates a reduction compared to that of IZO (44.67%). As a result, the stability of the IGZO TFT is improved compared to that of the IZO TFT, but the decrease in O<sub>II</sub> associated with the carrier concentration and increase in O<sub>III</sub> causing scattering cause a decrease in mobility. These results are consistent with the stress test results under various conditions shown in

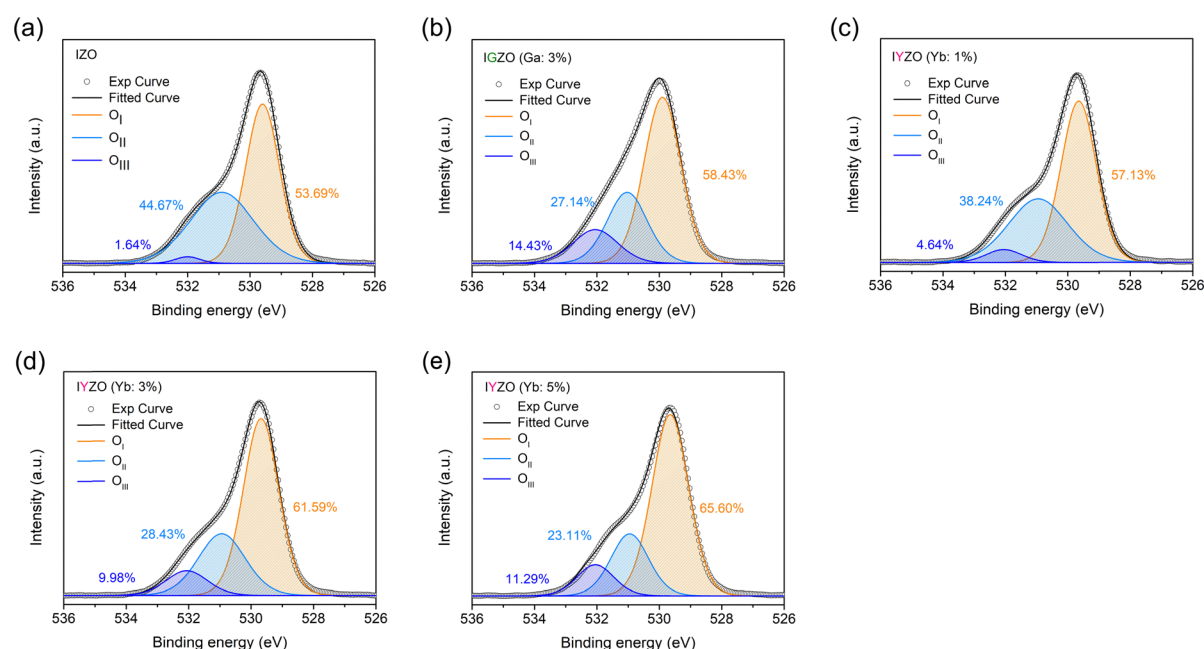


Fig. 5 XPS spectra of O 1s peaks for the chemical bonding states of the (a) IZO film, (b) IGZO (Ga: 3%) film and IYZO films with (c) Yb: 1%, (d) Yb: 3%, and (e) Yb: 5%, respectively.

Fig. 2(a) and 3. Fig. 5(c)–(e) demonstrate that as the doping concentration of Yb increases, the proportion of O<sub>I</sub> gradually increases and that of V<sub>O</sub> gradually decreases. This may have been caused by the doping of Yb with a high M–O dissociation energy, promoting M–O bonding in the thin film and thus reducing the amount of V<sub>O</sub>. In particular, the ratio of O<sub>I</sub> in the IYZO film was 61.59%, which was 12% higher than that of the IGZO film at 55.16%. This indicates that Yb is less prone to defect formation than Ga and facilitates M–O bonding more efficiently. In addition, the ratio O<sub>II</sub> in the IYZO film was 28.43%, which was 14% higher than that of the IGZO film, and the ratio of O<sub>III</sub> was 19% lower than that of IGZO. V<sub>O</sub> and impurities like M–OH cause charge-trapping at the channel/gate insulator interface, leading to device instability. This charge-trapping interferes with the current flow in the channel, thereby degrading the SS. As a result, the reduction of V<sub>O</sub> through Yb doping leads to a decrease in trap states, effectively improving the SS, as shown in Table 1. In addition, the IYZO TFT exhibits excellent stability compared to IGZO under bias stress tests such as NBS. In particular, deep level V<sub>O</sub> dissociates under illumination and donates an electron to the CBM, resulting in a large shift in  $V_{th}$ .<sup>30</sup> Therefore, these results suggest that the introduction of Yb helps improve the stability

under various operating conditions, especially under illumination (Fig. 3 and 4).

In amorphous oxide semiconductors, the presence of V<sub>O</sub> presents a trade-off, as it can not only enhance mobility but also introduce instability. This dual nature can be explained through two simple models: one involving shallow V<sub>O</sub> which is located near the conduction band minimum (CBM) and acts as a shallow donor, thereby contributing to increased electrical conductivity; and the other involving deep V<sub>O</sub>, which is positioned below the Fermi level and forms deep defect states, reducing the electrical stability. These deep defect states have been reported to play a crucial role in NBIS-induced instability, as they facilitate charge trapping and persistent photoconductivity effects, ultimately leading to a negative shift in threshold voltage.<sup>48</sup> Furthermore, the formation energy of deep V<sub>O</sub> varies depending on the doping elements and the composition of the oxide system.<sup>49,50</sup> Thus, since the formation of deep V<sub>O</sub> can influence the stability of oxide semiconductors, it is important to assess how favorable its formation is depending on the type of doping. To investigate this, we performed DFT calculations to compute deep V<sub>O</sub> in IZO, IGZO, and IYZO.

The deep V<sub>O</sub> model generated in amorphous IZO was consistent with prior literature,<sup>49</sup> as illustrated in Fig. 6(a). Fig. 6(b)

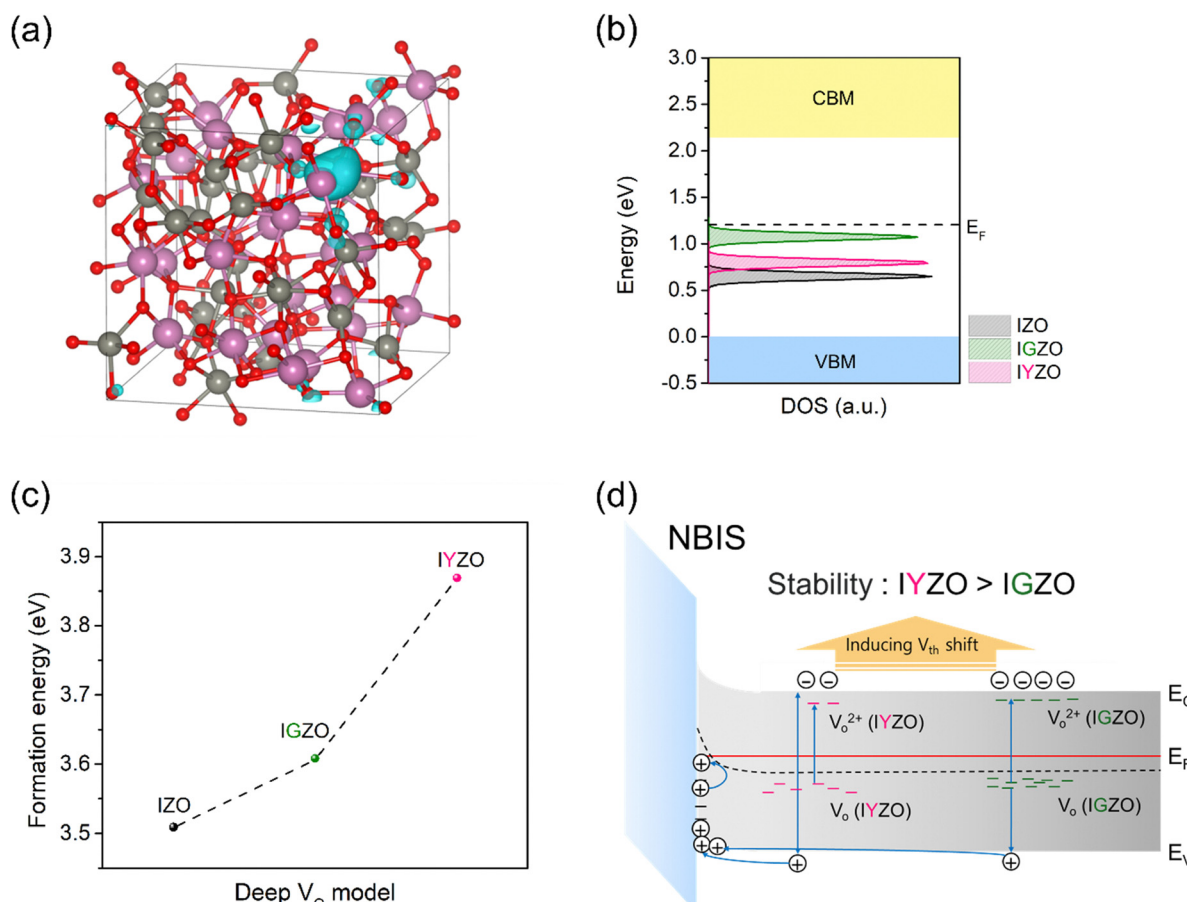


Fig. 6 (a) Deep V<sub>O</sub> model in a-IZO. (b) DFT-calculated density of states for IZO, IGZO, and IYZO where deep V<sub>O</sub> is present. The red, blue, and gray lines represent the energy states of the deep V<sub>O</sub> model for IGZO, IYZO, and IZO, respectively. (c) DFT-calculated formation energies of Deep V<sub>O</sub> in IZO, IGZO, and IYZO. (d) Schematic energy band diagram of the IYZO TFT and IGZO TFT under NBIS.

shows the density of states for IZO, IGZO, and IYZO where deep  $V_O$  is present. The energy states of deep  $V_O$  were found to be slightly below the Fermi level, confirming their nature as deep donors. The photoexcitation of this defect principally induces a negative shift of  $V_{th}$  under NBIS conditions.<sup>51,52</sup> Hence, the difference in energy states among these defects can serve as a comparative predictor for NBIS instability. The energy states of deep  $V_O$  were observed to decrease in the order IGZO, IYZO, and IZO, indicating that both Ga and Yb can improve NBIS instability. However, in a comparison between IGZO and IYZO, it was confirmed that the former would increase stability over the latter, which was inconsistent with our results. We hence conducted additional investigations on the thermodynamic formation behavior of deep  $V_O$ . Interestingly, the formation of deep  $V_O$  in IYZO was unfavorable compared to IGZO, as shown in Fig. 6(c). This prediction means a low concentration of deep  $V_O$  in IYZO, which aligns well with our XPS results. Consequently, we confirmed the heightened energy state of deep  $V_O$  as the origin of the enhanced NBIS instability in IYZO and IGZO. Additionally, we also identified that the lower

concentration of deep  $V_O$  in IYZO compared to IGZO supports its improved stability. Fig. 6(d) presents a schematic energy band diagram of IYZO TFTs and IGZO TFTs under NBIS, based on Fig. 6(a)–(c). Compared to IGZO, IYZO exhibits a higher formation energy for deep  $V_O$ , thereby reducing the formation of subgap defect states within the bandgap. Consequently, IYZO decreases the generation of electron-hole pairs induced by photoexcitation, which reduces the negative  $V_{th}$  shift and enhances the stability against NBIS. This is consistent with the stability test results presented in Fig. 3.

Fig. 7(a) presents the optical band gaps of the IZO, IGZO, and IYZO films. The optical band gap of IZO is 3.48 eV, that of IGZO is 3.50 eV, and those of IYZO (Yb: 1%), IYZO (Yb: 3%), and (Yb: 5%) are 3.46 eV, 3.48 eV, and 3.51 eV, respectively. Furthermore, the optical band gaps of IGZO (Ga: 1%) and IGZO (Ga: 5%) films are shown in Fig. S5 (ESI†), which were 3.49 and 3.51 eV, respectively. Fig. 7(b)–(h) demonstrate the results of the Gaussian fitting for the band edge states under the CBM. For N-type metal oxide films, the tail state near the CBM indicates the presence of defects in the film, and the absorption

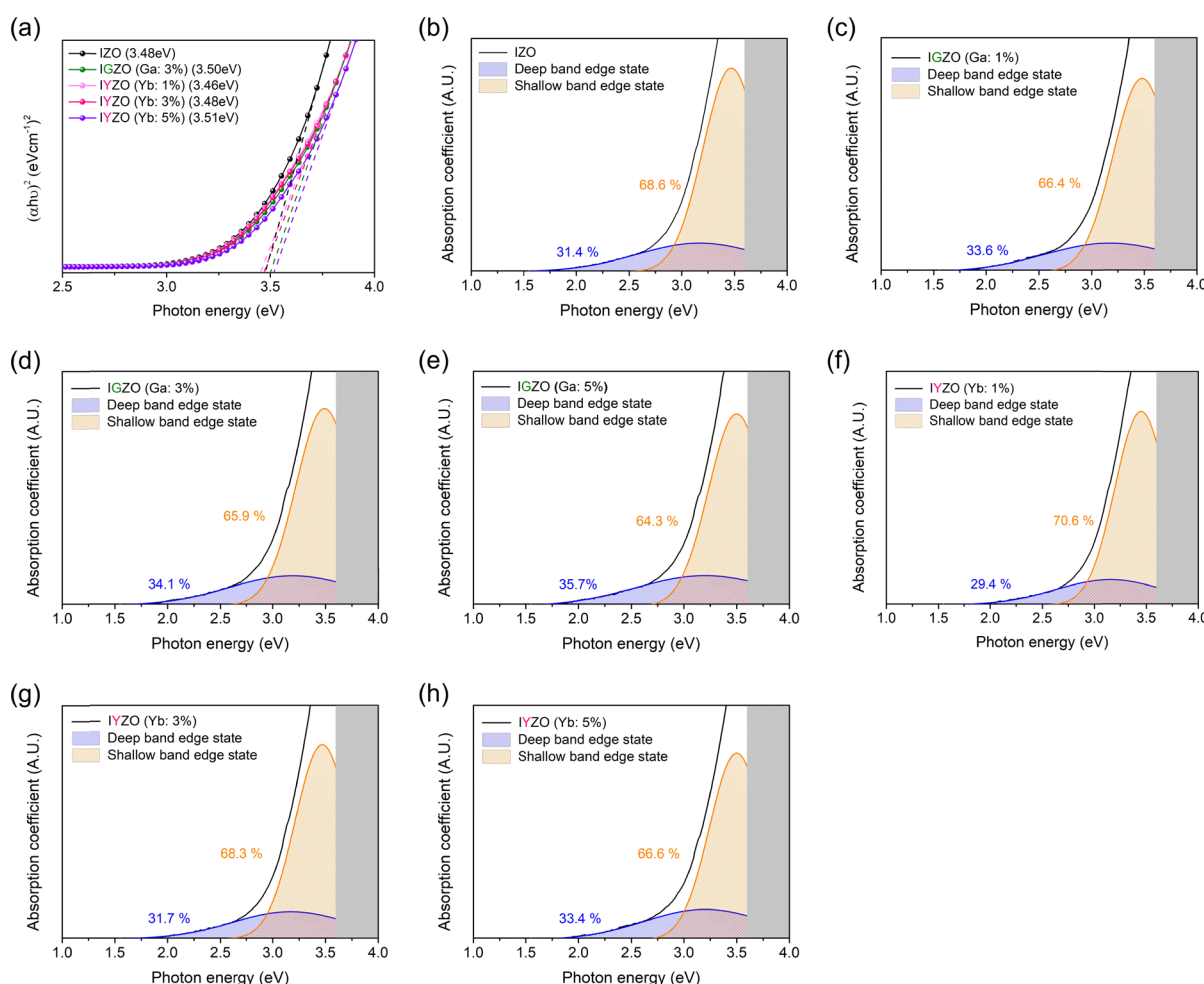


Fig. 7 (a) Tauc plot optical bandgaps calculated from UV-vis absorbance spectra for the IZO film, IGZO (Ga: 3%) film, and IYZO films with various Yb ratios. Band edge state below the conduction band minimum of the (b) IZO film, IGZO films with (c) Ga: 1%, (d) Ga: 3%, (e) Ga: 5%, IYZO films with (f) Yb: 1%, (g) Yb: 3%, and (h) Yb: 5%, respectively.

coefficient increases as the concentration of vacant electron trap levels within the bandgap increases.<sup>31</sup> In addition, shallow band edge states located near the edge of the CBM are associated with a carrier concentration by  $V_O$ , whereas deep band edge states are associated with scattering.<sup>53</sup> Therefore, the band edge state was divided into shallow and deep band edge states for fitting, the results of which were analyzed. A similar trend was observed, with the area ratio of the deep band edge states increasing as the composition of Ga and Yb in the thin film increased. The shallow band edge state of the IGZO (Ga: 1%) film was reduced by 2.2% compared to that of the IZO film, and that of the IGZO film was reduced by 2.7%. In contrast to IGZO films, the area of the shallow band edge states increased by 2% for the IYZO (Yb: 1%) film (70.6%) compared to that of the IZO film (68.6%). In addition, the shallow band edge state of the IYZO film was 68.3%, which was comparable to that of the IZO film. Fig. 2(e) demonstrates that the mobility of the IYZO (Yb: 1%) TFT ( $12.81 \text{ cm}^2 \text{ V}^{-1} \text{ s}^{-1}$ ) increases by 8% compared to that of the IZO TFT ( $11.83 \text{ cm}^2 \text{ V}^{-1} \text{ s}^{-1}$ ), whereas that of the IYZO TFT ( $12.22 \text{ cm}^2 \text{ V}^{-1} \text{ s}^{-1}$ ) increased by 3%,

indicating no decrease in mobility. Consequently, the electrical characteristics of IGZO/IYZO TFTs exhibit a trend consistent with the behavior of shallow band edge states.

Furthermore, compared to the IZO film, the increase in the area ratio of the deep band edge states of the IYZO and IGZO films is 0.3% and 2.7%, respectively, which was 9 times lower in the IYZO film. As this increase in the deep band edge states can lead to an increase in the generation of charge trapping in the subgap defect state, the IGZO TFTs apparently demonstrated lower stability than the IYZO TFTs under bias stress (Fig. 3). Furthermore, the significantly larger area ratio of deep band edge states of IGZO compared to IYZO, as shown in Fig. 6(c) and (d), is consistent with the results in Fig. 6(c) and (d), indicating the lower deep  $V_O$  formation energy of IGZO, leading to a higher concentration of deep  $V_O$ . Consequently, it can be confirmed that IYZO effectively suppresses the formation of defect states compared to IGZO, thereby enhancing stability.

Fig. 8(a)-(c) demonstrate the transmission line method (TLM) analyses, which were used to verify the electrical characteristics at the interface between the channel layer and

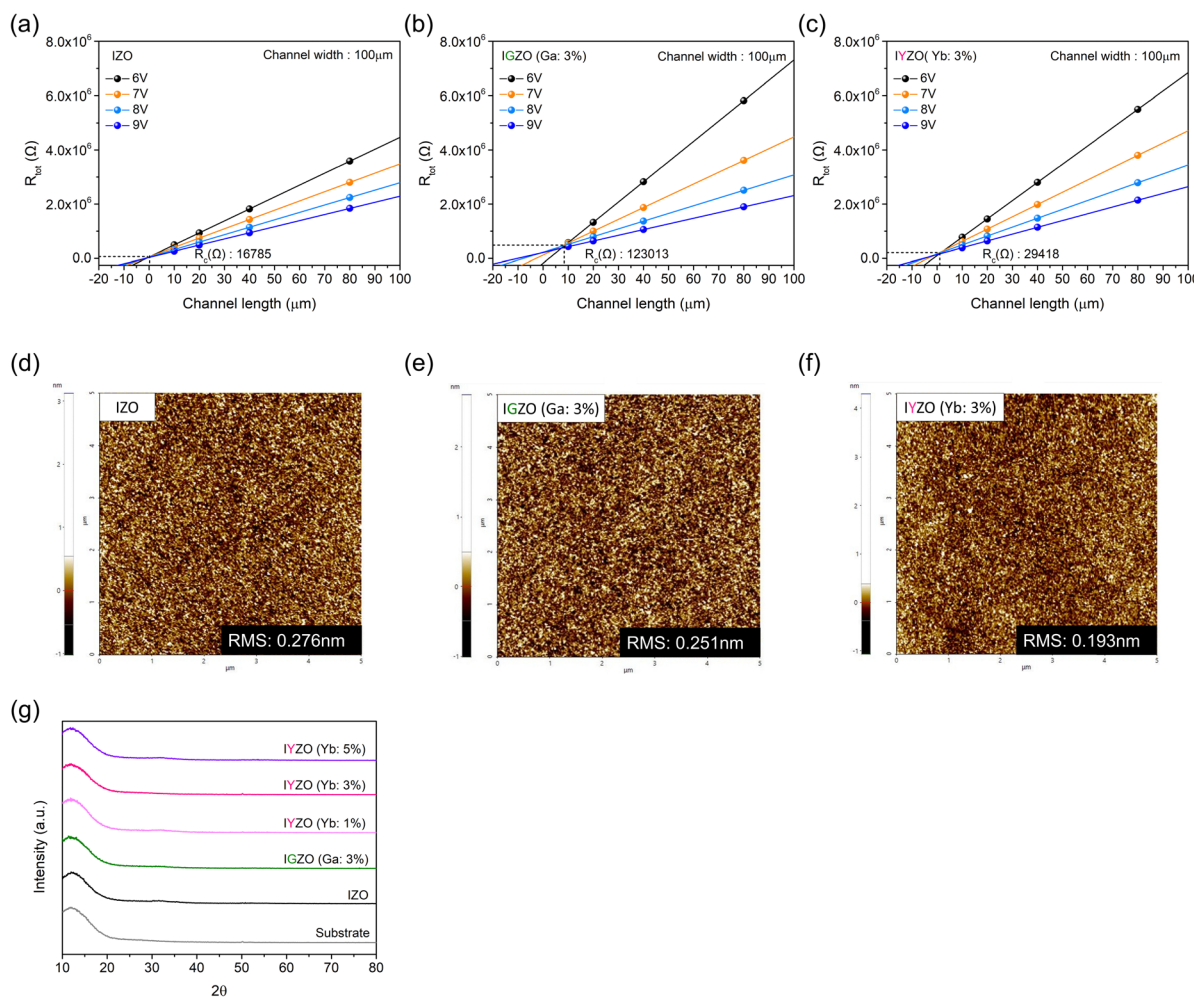


**Fig. 8** Contact resistance ( $R_c$ ) extraction using the TLM from the (a) IZO TFT, (b) IGZO (Ga: 3%) TFT and (c) IYZO (Yb: 3%) TFT, respectively. AFM images of (d) IZO film, (e) IGZO (Ga: 3%) film, and (f) IYZO (Yb: 3%) film, respectively. (g) GI-XRD patterns of the substrate, IZO film, IGZO (Ga: 3%) film, and IYZO films with various Yb concentrations.

source/drain as a function of Ga and Yb doping. The contact resistance ( $R_c$ ) of the IZO, IGZO, and IYZO films was extracted and plotted as a function of the channel length for different gate voltages. The channel width of the TFTs for the TLM analysis was fixed at 100  $\mu\text{m}$ , and the channel lengths were set to 10, 20, 40, and 80  $\mu\text{m}$ ; a gate voltage was applied at 6–9 V and the drain voltage was applied at 1.1 V. Compared to the IZO film,  $R_c$  increased when doping with Ga and Yb. In particular, the  $R_c$  value of the IGZO film increased 7 times compared to that of the IZO TFT, whereas the  $R_c$  of the IYZO TFT slightly increased by 1.75 times. When a large contact resistance exists between the channel layer and source/drain electrode, high bias must be applied to the S/D to inject carriers into the device, leading to poor mobility. Therefore, the TLM results have demonstrated that the IYZO TFT has lower contact resistance than the IGZO TFT, which significantly suppresses the decrease in the electrical characteristics. This is consistent with the result that the mobility of the IYZO TFT ( $12.22 \text{ cm}^2 \text{ V}^{-1} \text{ s}^{-1}$ ) is 18% higher than that of the IGZO TFT ( $10.34 \text{ cm}^2 \text{ V}^{-1} \text{ s}^{-1}$ ), as shown in Fig. 2(e). Fig. 8(d)–(f) demonstrate the roughness values of the IZO, IGZO, and IYZO films, respectively, and Fig. S6 (ESI<sup>†</sup>) presents the roughness values of the films under various doping concentrations of Ga/Yb. The root mean square (RMS) value of the IZO film was 0.275 nm, that of the IGZO film was 0.251 nm, and that of the IYZO film was 0.193 nm, indicating that the RMS values decreased after doping. In addition, the RMS values of the IGZO (Ga: 1%), IGZO (Ga: 5%), IYZO (Yb: 1%), and IYZO (Yb: 5%) films were 0.261, 0.236, 0.266, and 0.202 nm, respectively, which decreased as the doping content increased. This trend was similar to that observed in conventional amorphous semiconductors and may explain why the contact resistance of the IYZO film was lower than that of IGZO film.<sup>13</sup> Fig. 8(g) presents the GI-XRD pattern of IZO, IYZO, and IGZO films deposited on the Si substrate, indicating that all the films have an amorphous structure.

## 4. Conclusion

This study introduced Yb as a new dopant into IZO-based channel materials by a solution process and showed that IYZO TFT demonstrated a simultaneous improvement in the mobility and stability compared to the Ga-doped IGZO TFT. The mobility of the IYZO TFT was  $12.22 \text{ cm}^2 \text{ V}^{-1} \text{ s}^{-1}$ , which was comparable to that of the IZO TFT ( $11.83 \text{ cm}^2 \text{ V}^{-1} \text{ s}^{-1}$ ), and 18% better than that of the IGZO TFT ( $10.34 \text{ cm}^2 \text{ V}^{-1} \text{ s}^{-1}$ ). In particular, the IYZO TFT exhibited excellent stability under operating conditions with illumination. The photoresponse characteristics of the IYZO TFT improved by 29% compared to those of the IGZO TFT, and the value of  $\Delta V_{\text{th}}$  ( $-5.8 \text{ V}$ ) in the NBIS test is decreased by 24% compared to that of the IGZO TFT ( $-7.6 \text{ V}$ ). The XPS analysis revealed that the introduction of Yb can effectively suppress  $\Delta V_{\text{th}}$  during stress testing by controlling the formation of deep  $V_O$ , which caused trapping at the insulator and channel layer interface. Furthermore, the

IGZO film was confirmed to increase the deep band edge state compared to the IYZO film, which was demonstrated by analyzing the deep  $V_O$  formation energy via DFT calculations. As IYZO is expected to be a new candidate for replacing IGZO, various studies are being conducted to introduce a low-temperature annealing treatment process to apply to ultra-flexible displays.

## Data availability

The data supporting this article have been included as part of the ESI.<sup>†</sup>

## Conflicts of interest

There are no conflicts to declare.

## Acknowledgements

This research was supported by the National Research Foundation of Korea (NRF) funded by the Ministry of Science and ICT (NRF-2020M3H4A3081867) and supported by the Ministry of Trade, Industry and Energy (MOTIE) and Korea Institute for Advancement of Technology (KIAT) through the International Cooperative R&D program (P 0026102). This work was also supported by the Ceramic Strategic Research Program (PROJ25033-0-01) through the Korea Institute of Ceramic Engineering & Technology (KICET).

## References

- 1 K. Nomura, H. Ohta and A. Takagi, *et al.*, Room-temperature fabrication of transparent flexible thin-film transistors using amorphous oxide semiconductors, *Nature*, 2004, **432**, 488–492.
- 2 B. Lu, Z. Fei and Y. Zhao, *et al.*, Amorphous oxide semiconductors: From fundamental properties to practical applications, *Curr. Opin. Solid State Mater. Sci.*, 2023, **27**, 101092.
- 3 G. Goncalves, E. Elangovan and P. Barquinha, *et al.*, Influence of post-annealing temperature on the properties exhibited by ITO, IZO and GZO thin films, *Thin Solid Films*, 2007, **515**, 8562–8566.
- 4 J. Lee, J. Jin and S. Maeng, *et al.*, Enhancement of the Electrical Performance and Bias Stability of RF-Sputtered Indium Tin Zinc Oxide Thin-Film Transistors with Vertical Stoichiometric Oxygen Control, *ACS Appl. Electron. Mater.*, 2022, **4**, 1800–1806.
- 5 Y.-K. Liang, J.-W. Lin and L.-C. Peng, *et al.*, Electrical Characteristics of Ultrathin InZnO Thin-Film Transistors Prepared by Atomic Layer Deposition, *IEEE Trans. Electron Devices*, 2023, **70**, 1067.
- 6 H.-M. Kim, D.-G. Kim and Y.-S. Kim, *et al.*, Atomic layer deposition for nanoscale oxide semiconductor thin film transistors: review and outlook, *Int. J. Extreme. Manuf.*, 2023, **5**, 012006.

- 7 Q.-J. Sun, J. Wu and M. Zhang, *et al.*, Enhanced Electrical Performance and Bias-Stress Stability of Solution-Processed Bilayer Metal Oxide Thin-Film Transistors, *Phys. Status Solidi A*, 2022, **219**, 2200311.
- 8 H. J. Kim, J. Jung and H. J. Kim, Enhancement of electrical characteristics and stability of self-patterned In–Zn–O thin-film transistors based on photosensitive precursors, *Sci. Rep.*, 2020, **10**, 18853.
- 9 C. Avis, H. R. Hwang and J. Jang, Effect Of Channel Layer Thickness On The Performance Of Indium–Zinc–Tin Oxide Thin Film Transistors Manufactured By Inkjet Printing, *ACS Appl. Mater. Interfaces*, 2014, **6**, 10941–10945.
- 10 S. Cung, K. Cho and T. Lee, Recent Progress in Inkjet-Printed Thin-Film Transistors, *Adv. Sci.*, 2019, **6**, 1801445.
- 11 Z. Han, J. Han and A. Abiliz, Enhanced electrical performance of InGaSnO thin-film transistors by designing a dual-active-layer structure, *Appl. Surf. Sci.*, 2024, **648**, 158995.
- 12 K.-M. Jung, J. Oh and H. E. Kim, *et al.*, Stability improvement of solution-processed IGZO TFTs by fluorine diffusion from a CYTOP passivation layer, *J. Phys. D: Appl. Phys.*, 2020, **53**, 355107.
- 13 W. Cai, M. Li and H. Li, *et al.*, Significant performance and stability improvement of low-voltage InZnO thin-film transistors by slight La doping, *Appl. Phys. Lett.*, 2022, **121**, 062108.
- 14 Y. Zhu, Y. He and S. Jiang, *et al.*, Indium–gallium–zinc–oxide thin-film transistors: Materials, devices, and applications, *J. Semicond.*, 2021, **42**, 031101.
- 15 G. Baek, K. Abe and A. Kuo, *et al.*, Electrical Properties and Stability of Dual-Gate Coplanar Homojunction DC Sputtered Amorphous Indium–Gallium–Zinc–Oxide Thin-Film Transistors and Its Application to AM-OLEDs, *IEEE Trans. Electron Devices*, 2011, **58**, 4344–4353.
- 16 I. P. Park, B. K. Hwang and B. R. Lee, *et al.*, Threshold voltage tuning of IGZTO thin-film transistors deposited by RF sputtering for high-resolution flexible displays using deep ultraviolet light, *J. Mater. Chem. C*, 2023, **11**, 7793–7801.
- 17 J. Leppaniemi, K. Ojanpera and T. Kololuoma, *et al.*, Rapid low-temperature processing of metal-oxide thin film transistors with combined far ultraviolet and thermal annealing, *Appl. Phys. Lett.*, 2014, **105**, 113514.
- 18 R. N. Bukke, N. N. Mude and M. M. Islam, *et al.*, Improvement of metal-oxide films by post atmospheric Ar/O<sub>2</sub> plasma treatment for thin film transistors with high mobility and excellent stability, *Appl. Surf. Sci.*, 2021, **568**, 150947.
- 19 Y. Chen, Z. He and Y. Li, *et al.*, Regulation of precursor solution concentration for In-Zn oxide thin film transistors, *Curr. Appl. Phys.*, 2018, **18**, 1300–1305.
- 20 R. A. John, A. C. Nguyen and Y. Chen, *et al.*, Modulating Cationic Ratios for High-Performance Transparent Solution-Processed Electronics, *ACS Appl. Mater. Interfaces*, 2016, **8**, 1139–1146.
- 21 H. Kim, S. Maeng and S. Lee, *et al.*, Improved Performance and Operational Stability of Solution-Processed InGaSnO (IGTO) Thin Film Transistors by the Formation of Sn–O Complexes, *ACS Appl. Electron. Mater.*, 2021, **3**, 1199–1210.
- 22 T.-T. Yang, D.-H. Kuo and K.-P. Tang, n-type Sn substitution in amorphous IGZO film by sol-gel method: A promoter of hall mobility up to 65 cm<sup>2</sup>/V s, *Non-Cryst. Solids*, 2021, **553**, 120503.
- 23 Y. J. Kim, S. Oh and B. S. Yang, *et al.*, Impact of the Cation Composition on the Electrical Performance of Solution-Processed Zinc Tin Oxide Thin-Film Transistors, *ACS Appl. Mater. Interfaces*, 2014, **6**, 14026–14036.
- 24 W. S. Choi, H. Jo and M. S. Kwon, *et al.*, Control of electrical properties and gate bias stress stability in solution-processed a-IZO TFTs by Zr doping, *Curr. Appl. Phys.*, 2014, **14**, 1831–1836.
- 25 D.-Y. Zhong, J. Li and C.-Y. Zhao, *et al.*, Enhanced Electrical Performance and Negative Bias Illumination Stability of Solution-Processed InZnO Thin-Film Transistor by Boron Addition, *IEEE Trans. Electron Devices*, 2018, **65**, 520–525.
- 26 J. Liu, H. Xu and M. Li, *et al.*, Comprehensive Study of Improved Negative-Bias-Illumination-Temperature Stress Stability in Terbium-Doped Indium-Zinc-Oxide Thin-Film Transistors, *IEEE Trans. Electron Devices*, 2023, **70**, 3563–3568.
- 27 T. Jun, K. Song and Y. Jung, *et al.*, Bias stress stable aqueous solution derived Y-doped ZnO thin film transistors, *J. Mater. Chem.*, 2011, **21**, 13524–13529.
- 28 S.-P. Baek, J.-H. Kim and T.-J. Lee, *et al.*, Tantalum Doping to Improve Switching Characteristics and Bias Stress Stability of Amorphous Indium-Gallium-Zinc Oxide Thin-Film Transistors, *ECS J. Solid State Sci. Technol.*, 2021, **10**, 065004.
- 29 P. Barquinha, G. Goncalves and L. Pereira, *et al.*, Effect of annealing temperature on the properties of IZO films and IZO based transparent TFTs, *Thin Solid Films*, 2007, **515**, 8450–8454.
- 30 H. Oh, S.-M. Yoon and M. K. Ryu, *et al.*, Photon-accelerated negative bias instability involving subgap states creation in amorphous In–Ga–Zn–O thin film transistor, *Appl. Phys. Lett.*, 2010, **97**, 183502.
- 31 J. Socratos, K. K. Banger and Y. Vaynzof, *et al.*, Electronic Structure of Low-Temperature Solution-Processed Amorphous Metal Oxide Semiconductors for Thin-Film Transistor Applications, *Adv. Funct. Mater.*, 2015, **25**, 1873–1885.
- 32 S. Hwang, J. H. Lee and C. H. Woo, *et al.*, Effect of annealing temperature on the electrical performances of solution-processed InGaZnO thin film transistors, *Thin Solid Films*, 2011, **519**, 5146–5149.
- 33 Y.-R. Luo, *Comprehensive Handbook of Chemical Bond Energies*, CRC Press, Boca Raton, 2007, p. 1688.
- 34 Z. Wang, T. Zhao and J. Li, *et al.*, Solution-Processed High Performance Ytterbium-Doped In<sub>2</sub>O<sub>3</sub> Thin Film Transistor and Its Application in Common-Source Amplifier, *IEEE Trans. Electron Devices*, 2023, **70**, 1073–1078.
- 35 W. Xu, C. Xu and L. Hong, *et al.*, Aqueous Solution-Processed Nanometer-Thin Crystalline Indium Ytterbium Oxide Thin-Film Transistors, *Nanomaterials*, 2022, **12**, 1216.
- 36 G. Kresse and J. Furthmüller, Efficient iterative schemes for ab initio total-energy calculations using a plane-wave basis set, *Phys. Rev. B: Condens. Matter Mater. Phys.*, 1996, **54**, 11169.

- 37 G. Kresse and J. Furthmuller, Efficiency of ab-initio total energy calculations for metals and semiconductors using a plane-wave basis set, *Comput. Mater. Sci.*, 1996, **6**, 15–50.
- 38 P. E. Blochl, Projector augmented-wave method, *Phys. Rev. B: Condens. Matter Mater. Phys.*, 1994, **50**, 17953.
- 39 J. P. Perdew, B. Burke and M. Ernzerhof, Generalized Gradient Approximation Made Simple, *Phys. Rev. Lett.*, 1997, **78**, 1396.
- 40 A. D. Becke and E. R. Johnson, A simple effective potential for exchange, *J. Chem. Phys.*, 2006, **124**, 221101.
- 41 F. Tran and P. Blaha, Accurate Band Gaps of Semiconductors and Insulators with a Semilocal Exchange-Correlation Potential, *Phys. Rev. Lett.*, 2009, **102**, 226401.
- 42 B. Deng, P. Zhong and K. Jun, *et al.*, CHGNet as a pretrained universal neural network potential for charge-informed atomistic modelling, *Nat. Mach. Intell.*, 2023, **5**, 1031–1041.
- 43 H. Xu, M. Xu and M. Li, *et al.*, Trap-Assisted Enhanced Bias Illumination Stability of Oxide Thin Film Transistor by Praseodymium Doping, *ACS Appl. Mater. Interfaces*, 2019, **11**, 5232–5239.
- 44 A. Abliz, D. Wan and L. Yang, *et al.*, Investigation on the electrical performances and stability of W-doped ZnO thin-film transistors, *Mater. Sci. Semicond. Process.*, 2019, **95**, 54–58.
- 45 D. Wan, X. Liu and A. Abliz, *et al.*, Design of Highly Stable Tungsten-Doped IZO Thin-Film Transistors With Enhanced Performance, *IEEE Trans. Electron Devices*, 2018, **65**, 1018–1022.
- 46 G.-W. Chang, T.-C. Chang and J.-C. Jhu, *et al.*, Temperature-Dependent Instability of Bias Stress in InGaZnO Thin-Film Transistors, *IEEE Trans. Electron Devices*, 2014, **61**, 2119–2124.
- 47 J. Park, Y. S. Rim and C. Li, *et al.*, Defect-induced instability mechanisms of sputtered amorphous indium tin zinc oxide thin-film transistors, *J. Appl. Phys.*, 2018, **123**, 161568.
- 48 T. Kamiya, K. Nomura and H. Hosono, Electronic structure of the amorphous oxide semiconductor a-InGaZnO<sub>4-x</sub>: Tauc–Lorentz optical model and origins of subgap states, *Phys. Status Solidi A*, 2009, **206**, 860–867.
- 49 H. Song, G. Kang and Y. Kang, *et al.*, The Nature of the Oxygen Vacancy in Amorphous Oxide Semiconductors: Shallow Versus Deep, *Phys. Status Solidi B*, 2019, **256**, 1800486.
- 50 J. Lee, C. H. Choi and T. Kim, *et al.*, Hydrogen-Doping-Enabled Boosting of the Carrier Mobility and Stability in Amorphous IGZTO Transistors, *ACS Appl. Mater. Interfaces*, 2022, **14**, 57016–57027.
- 51 B. Ryu, H.-K. Noh and E.-A. Choi, *et al.*, O-vacancy as the origin of negative bias illumination stress instability in amorphous In–Ga–Zn–O thin film transistors, *Appl. Phys. Lett.*, 2010, **97**, 022108.
- 52 J. K. Jeong, Photo-bias instability of metal oxide thin film transistors for advanced active matrix displays, *J. Mater. Res.*, 2013, **28**, 2071–2084.
- 53 A. Song, H.-W. Park and H.-D. Kim, *et al.*, Significant enhancement of the bias stability of Zn-O-N thin-film transistors via Si doping, *Sci. Rep.*, 2020, **10**, 719.